Aggregation and counterion condensation in solution of charged proteinlike copolymers: A molecular-dynamics study

ARTICLE *in* THE JOURNAL OF CHEMICAL PHYSICS · JULY 2003

Impact Factor: 2.95 · DOI: 10.1063/1.1579683

Aggregation and counterion condensation in solution of charged proteinlike copolymers: A molecular-dynamics study

Pavel G. Khalatur[a)]
Department of Polymer Science, University of Ulm, Ulm D-89069, Germany

Alexei R. Khokhlov
Department of Polymer Science, University of Ulm, Ulm D-89069, Germany and Physics Department, Moscow State University, Moscow 117234, Russia

Dmirtii A. Mologin
Department of Physical Chemistry, Tver State University, Tver 170002, Russia

Peter Reineker
Department of Theoretical Physics, University of Ulm, Ulm D-89069, Germany

(Received 5 March 2003; accepted 14 April 2003)

We present the results of molecular dynamics simulations of charged proteinlike hydrophobic–hydrophilic ($\mathcal{HP}$) copolymers with a fixed charge distribution under pure solvent conditions. The processes of coil-to-globule transition, aggregation of polymer globules, and counterion condensation are studied in detail as a function of temperature. Various static structure factors and pair correlation functions, that occur in polyelectrolyte solutions, are also analyzed. Our simulations show that the chains pass through strong conformational changes while changing temperature. We find three different temperature regimes which are characterized by a different behavior of Coulomb energy, chain sizes, and pair correlation functions. In the high-temperature regime, at the reduced temperature $T>3.0$, the chains have an extended conformation with many hydrophobic blobs. As temperature is decreased, one observes a counterion condensation and sharp decrease in chain size. In this regime, we observe a solution of nonaggregating polymer globules which form a stable array resembling a charge-stabilized (micro)suspension or microgel phase. A further decrease in temperature (at $T<0.5$) leads to an aggregation of the isolated globules which form aggregates built up from individual globules connected by a layer of counterions condensed on the globular surface. It is found that the transitions between the temperature regimes are thermodynamically reversible.
 [DOI: 10.1063/1.1579683]

I. INTRODUCTION

A variety of synthetic and biological macromolecules are polyelectrolytes. The most well-known polyelectrolyte biopolymers (proteins, DNA, and RNA) are responsible in living systems for functions which are incomparably more complex and diverse than the functions usually discussed for synthetic copolymers.[1] As a simplest example, it is well-known that the functioning of globular proteins depends on two main factors: (i) They are globular and (ii) they are soluble in an aqueous medium. It should be noted that the combination of these two factors is nontrivial, e.g., for homopolymers and random copolymers the transition to globular conformation is usually accompanied by the precipitation of globules from the solution.[2,3] In a dilute solution, protein globules are soluble because of the special primary sequence: In the native conformation most of hydrophobic amino acids are in the core of the globule while hydrophilic and charged amino acids form the envelope of this core. At nonzero concentrations, depending on temperature, *p*H, presence and kind of salt, etc., individual proteins may remain stable in the isolated native state, may aggregate preserving their globular native state or aggregate changing their native conformation (the so-called prionlike behavior).[1] The two latter aspects can be neglected in extremely dilute solutions, but they are certainly important, e.g., for *in vitro* or computer design of new (soluble) proteinlike copolymers. Specifically, the aggregation has been found to increase with increasing protein concentration, decreasing protein net charge, and increasing content of salt.[1–3]

Recently,[4–6] we proposed the idea of the conformation-dependent sequence design of two-letter copolymers consisting of monomer units of two sorts. This approach includes the generation of a special primary sequence in two-letter copolymers from some specific conformation of a homopolymer chain (''parent'' conformation) via a ''coloring procedure'' of the instant image of such chain. In Refs. 4–6, this idea was realized for the case when the parent conformation corresponds to a dense globule of a homopolymer chain: the monomer units lying in the core of such globule were designated as $\mathcal{H}$ units and called hydrophobic, while the monomer units belonging to the surface of the ''instant image'' of a globule were designated as $\mathcal{P}$ units and called hydrophilic. In this way we generated the so-called ''proteinlike copolymers.'' Further studies of the properties of such copolymers have shown that their behavior is essentially different from

a)Electronic mail: khalatur@germany.ru

that of the random copolymers with the same $\mathcal{HP}$ composition, and random-block copolymers with the same $\mathcal{HP}$ composition and the same ''degree of blockiness.''[7–11] In particular, the coil-globule transition in proteinlike $\mathcal{HP}$ copolymers occurring under gradual increase of the attraction of $\mathcal{H}$ units takes place at higher temperatures, is more abrupt, and has faster kinetics, as compared to random and random-block copolymers with the same $\mathcal{HP}$ composition and the same ''degree of blockiness.'' We concluded that the reason for this is that the proteinlike copolymer ''inherits'' (or ''memorizes'') some of the properties of the parent globule, in particular, the existence of a well-formed pure $\mathcal{H}$ core coupled with a stabilizing $\mathcal{P}$ envelope. These properties are then manifested in other conditions, making the dense globule self-assembly easier to be realized. Also, both exact analytical theory and computer simulations showed that the statistical properties of designed proteinlike sequences are characterized by a specific long-range correlation obeying the so-called Levy-flight statistics.[12] Later, proteinlike $\mathcal{HP}$ copolymers were synthesized in real chemical experiments,[13,14] and the above-mentioned predictions of computer experiments were confirmed. The role of ''coloring'' in real experiments is played by the reaction of a monomer unit with a reagent, which converts hydrophobic unit to a charged or polar group.

Until now computer studies focused on single proteinlike copolymers consisting of uncharged (electroneutral) monomer units.[4–11] It is known, however, that real proteins are built up both from hydrophobic and polar amino acid residues, some of the latter are charged.[1] Many of the conformational and collective properties of proteins are due to a complex interplay between short-range (hydrophobic) effects and long-range (Coulomb) interactions. In particular, the unique solution properties of globular proteins (e.g., their aggregative stability in an aqueous medium) are determined by electrostatic effects.[1–3] Thus, the understanding of the behavior of charged designed copolymers in solution is of primary interest. To this end, in the present article we will use the method of molecular dynamics to simulate a primitive model of salt-free solutions of charged proteinlike copolymers with monovalent counterions.

This study will also address some of the general issues raised for solutions of polyelectrolytes at nonzero concentrations. There have been a number of computer simulation studies on the static behavior and dynamics of polyelectrolyte solutions.[15–24] Most attention has focused on the equilibrium conformations of strongly charged homopolymer chains dissolved both in good and poor solvents in the low-concentration limit. In particular, it was shown that strongly charged hydrophobic chains in poor enough solvents can undergo coil-to-globule transition.[16–18] Currently, however, no detailed understanding of the structure of the collapsed state exists. Micka *et al.*[23,24] have simulated the multichain polyelectrolyte system consisting of the flexible chains with alternating charged and electroneutral monomer units.

Contrary to the papers,[15–24] we will focus the discussion in this paper on the stability of polyelectrolytes towards aggregation. Although our consideration will deal with copolymers having proteinlike statistics, we believe that most of the conclusions should remain valid in the general case. To summarize, in the present paper, using molecular-dynamics simulations, we will consider the behavior of proteinlike copolymers with charged monomer units in a solution. Our aim is to study conformations of such copolymers, as well as their stability towards aggregation under poor solvent conditions for hydrophobic monomer units.

II. MODEL AND SIMULATION TECHNIQUE

The system under consideration is a dilute solution of $\mathcal{N}$-unit polyelectrolyte chains with a fixed charge distribution and oppositely charged small mobile counterions. There is no additional salt in the system. The solvent (water) is replaced by a dielectric background and a heat bath.

We consider a model of a flexible copolymer chain that involves only two types of monomer units, $\mathcal{H}$ (hydrophobic) and $\mathcal{P}$ (hydrophilic or polar). The $\mathcal{P}$ units are assumed to be negatively charged, while $\mathcal{H}$ units are electroneutral. The $\mathcal{HP}$ composition is fixed at 1:1. We employ a continuum space (bead-rod) model, as opposed to widely used lattice $\mathcal{HP}$ models,[25,26] since the latter have intrinsically discretized dynamics of a rather arbitrary nature and have slow relaxation for a dense globular state. The time evolution of the system is determined by Newton's equations that are solved by using the method of molecular dynamics (MD). Monomer units (chain beads) are linked by rigid bonds of a fixed length to form a linear $\mathcal{HP}$ copolymer chain of length $\mathcal{N}$.

The two-particle potential energy of the system is given by

$$U=\sum_{i}^{N}\sum_{j\neq i}^{N}\left[U_{ev}(r_{ij})+U_{a}(r_{ij})+U_{C}(r_{ij})\right], \tag{1}$$

where N is the total number of particles (monomer units plus counterions) in the system, U_{ev} takes into account excluded volume and models the situation of a polymer in a good solvent, U_a characterizes attractive (hydrophobic) interactions between monomers of the chains, U_C is the energy of electrostatic interaction between charged particles ($\mathcal{P}$ monomer units and/or counterions). The distance between the particles i and j is defined as $r_{ij}=|\mathbf{r}_i-\mathbf{r}_j|$, where $\mathbf{r}_i$ denotes the position vector of particle i in three-dimensional space.

Excluded volume between any nonbonded particles (chain beads and counterions) is included via a repulsive Lennard-Jones (RLJ) potential

$$U_{ev}(r_{ij})=\begin{cases}4\epsilon\left[\left(\dfrac{\sigma}{r_{ij}}\right)^{12}-\left(\dfrac{\sigma}{r_{ij}}\right)^{6}+\dfrac{1}{4}\right], & r_{ij}\leqslant r_0,\\ 0, & r_{ij}>r_0.\end{cases} \tag{2}$$

where $\sigma=\epsilon=1$ and $r_0=2^{1/6}\sigma$ is a cut-off distance. The normalized parameter ϵ entering this equation controls the energy scale, whereas σ determines the interaction length between particles.

In addition to the excluded volume potential (2), the nonbonded beads interact via a Yukawa-type potential, for which we use the following simple form:

$$U_a(r_{ij})=\begin{cases} -\dfrac{\epsilon_{\alpha\beta}\sigma}{r_{ij}}\left[1-\left(\dfrac{r_{ij}}{r_c}\right)^2\right]^2, & r_0<r_{ij}\leqslant r_c, \\ 0, & r_{ij}>r_c. \end{cases} \tag{3}$$

In the model, this potential describes short-range hydrophobic intra- and interchain interactions. The parameter $\epsilon_{\alpha\beta}$ $(=\epsilon_{\mathcal{HH}},\epsilon_{\mathcal{PP}},\epsilon_{\mathcal{HP}})$ sets the depth of the minimum of the nonlocal attraction and $r_c=2.8\sigma$ is the cutoff distance for attractive interactions. The characteristic energy of $\mathcal{H}$–$\mathcal{H}$, $\mathcal{H}$–$\mathcal{P}$, and $\mathcal{P}$–$\mathcal{P}$ interactions is fixed at $\epsilon_{\mathcal{HH}}=\epsilon_{\mathcal{HP}}=\epsilon_{\mathcal{PP}}=2$ (all the energies are measured in units of k_BT). For $\epsilon_{\alpha\beta}=0$, there is no attraction between chain sites. The nature of hydrophobic forces is complicated, but for the purpose of the present study it is sufficient to introduce a nonspecific short-range attraction using potential (3) in which parameters are chosen to promote the collapse of the chains.

It is well-known that the electrostatic forces between charged species form the most basic element in any detailed theoretical model describing a polyelectrolyte solution. For a system of N particles with charges q_i at positions $\mathbf{r}_i$ in a cubic simulation cell of length L with periodic boundary conditions, the long-range Coulomb energy is given by

$$U_C=\frac{1}{4\pi\epsilon_0\epsilon_r}\sum_{\mathbf{m}}\sum_{i\neq j}^{N}\frac{q_iq_j}{|\mathbf{r}_{ij}+\mathbf{m}L|}, \tag{4}$$

where $\mathbf{r}_{ij}=\mathbf{r}_i-\mathbf{r}_j$, q_i is the charge of a given particle, ϵ_0 denotes the permittivity of free space, ϵ_r is the relative permittivity of the medium, and the sum over $\mathbf{m}$ takes into account the periodic images of the charged particles [$\mathbf{m}$ is an integer triple identifying a particular image cell; $\mathbf{m}=(0;0;0)$ indicates the ''real'' simulation cell, and all other cells are identified by their displacement from the central cell]. The charges on polyions and counterions, expressed in units of the elementary charge e, are equal to -1 and $+1$, respectively. Since in our simulations all charges are treated explicitly, electrostatic interactions are described by the electrostatic potentials (4) with a dielectric permittivity $\epsilon_r=1$. The slowly and conditionally convergent sums of Eq. (4) can be recast as two rapidly converging sums, one in real space ($\mathbf{r}$) and one in reciprocal space ($\mathbf{k}$). Employing the Ewald representation[27,28] for the electrostatic energy, this sum can be written in the following way: $U_C=U^{(r)}+U^{(k)}+U^{(s)}$, where $U^{(r)}$ is the contribution from real space, $U^{(k)}$ is the contribution from reciprocal (Fourier) $\mathbf{k}$-space, and $U^{(s)}$ denotes the so-called self energy term. To take into account long-range electrostatic interactions between charges, we use the highly optimized particle mesh Ewald (PME) method[29,30] in the SPME version presented in Ref. 30 and the fast Fourier transform (FFT) algorithm. The truncation distance for electrostatic interactions is set to $R_c=10\sigma$, and long-range corrections to the potential energy and pressure are made. The Ewald convergence parameter is $\alpha=0.3766\sigma^{-1}$. The order of B-splines is $n_B=5$ for all systems. The number of grid points in each direction is 72. These parameters ensure consistency between the Coulomb energy obtained through the pair potential and the Coulomb energy calculated through the virial.

Explicitly, no solvent particles are included in the simulations; that is, the solvent is represented by a dielectric continuum. In order to simulate solvation effects and the time evolution of the solution in contact with a heat bath of temperature T, we augment the equations of motion by Langevin uncorrelated noise terms.[28] In the MD simulations, the equations of motion of a polymer system in the presence of fixed constraints (the bead–rod model) are

$$m_i\ddot{\mathbf{r}}_i=-\nabla_i\left[U(\mathbf{r})-\sum_{s=1}^{n(\mathcal{N}-1)}\lambda_sG_s(\mathbf{r}_1,\ldots,\mathbf{r}_{n\mathcal{N}})\right] -\Gamma_i\dot{\mathbf{r}}_i+\mathbf{R}_i, \quad i=1,2,\ldots,N, \tag{5}$$

with the constraints of fixed bond lengths

$$\mathcal{G}_s(\mathbf{r}_1,\ldots,\mathbf{r}_{n\mathcal{N}})\equiv\tfrac{1}{2}[(\mathbf{r}_{s+1}-\mathbf{r}_s)^2-b^2]=0, \quad s=1,2,\ldots,\mathcal{N}-1,\ldots,n(\mathcal{N}-1), \tag{6}$$

where n is the number of chains in the system, $m_i=1$ is the mass of the chain bead or counterion i, $-\nabla_iU(\mathbf{r})$ represents the total nonbonded forces on the particle i, $b=\sigma$ is the bond length, λ_s's are the Lagrange multipliers, $\mathbf{R}_i$ describes the random force of the heat bath acting on particle i, and Γ takes into account the viscosity of the solvent. The summation in Eq. (5) is performed over all the $n(\mathcal{N}-1)$ bonds of the $\mathcal{N}$-unit polymer chains. This term represents the forces, $\nabla_i\Sigma_{s=1}^{n(\mathcal{N}-1)}\lambda_sG_s(\mathbf{r}_1,\ldots,\mathbf{r}_{n\mathcal{N}})$, which are due to the bond reactions.[31] Each of the sth geometrical constraint (bond) is associated with exactly one unknown λ_s. In Eq. (5), $\mathbf{R}_i$ and Γ_i are connected through the fluctuation–dissipation theorem, $\langle R_{\alpha i}(0)\cdot R_{\alpha i}(t)\rangle=2\Gamma_ik_BT\delta(t)$ ($\alpha=x,y,z$; T is the reference temperature), and ensures that the temperature is kept constant. Note that if Γ_i is included without the $\mathbf{R}_i$ term, the system would simply dissipate and no temperature effects could be addressed.

We take the parameter Γ to be dependent on solvent-accessible surface areas (SASA). To find the values of SASA for a given configuration, we perform an analytical computation of the surface areas $\mathcal{A}_i$ for each specified particle.[32,33] Having $\mathcal{A}_i$, one can define Γ_i as $\Gamma_i=\Gamma_0\mathcal{A}_i/\mathcal{A}_{\max}$, where $\mathcal{A}_{\max}$ is the maximum solvent-accessible surface area of a particle for the model under study and the reference value of Γ_0 is taken to be equal to unity. The weighting factor $\mathcal{A}_i/\mathcal{A}_{\max}$ represents the degree of exposure of the particle i to the solvent. When the value of SASA for a given particle is zero, the frictional and random forces are zero and the Langevin equation (5) reduces to Newton's equation of motion. For the chain in a globular conformation, this typically happens when the monomer unit is located in the core of a globule. On the contrary, a monomer unit located at the globular surface is strongly solvated; it means that $\mathcal{A}_i$ should be close to $\mathcal{A}_{\max}$ and, as a result, the value of Γ_i is close to its reference value Γ_0. In the following, the reference temperature T (measured in units of ϵ/k_B) is considered as main variable parameter.

The equations of motion (5) in conjunction with Eqs. (6) are solved iteratively using a Newtonian iteration procedure with the time step $\Delta t=0.01\sigma\sqrt{m/\epsilon}$. For this calculation we use the RATTLE algorithm.[31]

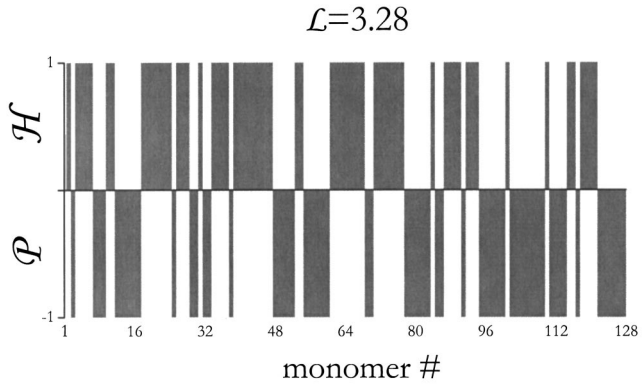

FIG. 1. Distributions of $\mathcal{H}$ and $\mathcal{P}$ monomeric units along the chain of proteinlike copolymer with average block length $\mathcal{L}=3.28$. In this figure, the $\mathcal{H}$ units are denoted as $+1$ and the $\mathcal{P}$ units as -1. The chain length is $\mathcal{N}=128$.

In order to obtain single proteinlike $\mathcal{HP}$ copolymer, the following computational strategy is employed:

(i) A self-avoiding homopolymer chain with uncharged $\mathcal{H}$ units is randomly generated;

(ii) the folding of the chain is performed at $\epsilon_{\mathcal{HH}}=2$ and $T=1$. Then this conformation is equilibrated for $\tau_1=4\times10^5$ integration time steps. As a result, we obtain a dense homopolymer globule;

(iii) one-half of the monomer units, having the largest solvent-accessible surface areas, SASA, and simultaneously well-separated from the center-of-mass of the globular core, are transformed into $\mathcal{P}$ type; the remaining monomer units with the (minimum) values of SASA and being closer to the center-of-mass of the globular core are considered to be of $\mathcal{H}$ type. Thus, the composition of the polymer sequence is constrained so that there are $\mathcal{N}/2$ hydrophobic and $\mathcal{N}/2$ hydrophilic monomer units and the primary structure of the heteropolymer is frozen. As a result, we obtain a bare proteinlike heteropolymer globule having a core-shell structure (see also Refs. 4–12).

The primary structure of a two-letter $\mathcal{HP}$ copolymer can be characterized by its composition, by the average lengths of the hydrophobic and hydrophilic blocks, $\mathcal{L}_{\mathcal{H}}$ and $\mathcal{L}_{\mathcal{P}}$, and by the specific distribution of $\mathcal{H}$ and $\mathcal{P}$ units along the chain. For the 128-unit copolymer generated in this work, we find $\mathcal{L}_{\mathcal{H}}\approx\mathcal{L}_{\mathcal{P}}=\mathcal{L}=3.28$. In Fig. 1 we present the distribution of $\mathcal{H}$ and $\mathcal{P}$ monomers along the chain of the proteinlike copolymer. From the comparison of the primary structures of proteinlike and random copolymers having the same $\mathcal{HP}$ composition we can see that the average lengths of $\mathcal{H}$ and $\mathcal{P}$ blocks in the proteinlike copolymer are longer. Indeed, for an infinitely long random copolymer, one has: $\mathcal{L}=2$. Thus, the primary structure emerging in the case of proteinlike copolymer can be characterized as ''random with long-range correlations'' (for more detail, see Ref. 12).

The bare globule was replicated 29 times. The identical images of the bare globule were initially placed on a regular simple cubic lattice spanning a periodic MD box without overlap between them and then were randomly reoriented. In subsequent calculations, each $\mathcal{P}$ monomer unit is assumed to be negatively charged, while $\mathcal{H}$ units are electroneutral. Then, univalent positively charged counterions were distributed in the box and the system constructed in this way was relaxed for a long time. At this initial stage, velocities were rescaled at each time–step to compensate for the large amount of heat produced in the system.

For computational efficiency, chains with relatively short length, $\mathcal{N}=128$, are used for most of the calculations. The cubic computational box with periodic boundary conditions contains $n=29$ polyions (total number of chain beads $n\mathcal{N}=3712$) and $n_c=1856$ counterions to ensure electroneutrality of the system. The entire system of n chains plus n_c counterions is enclosed in a periodic cubic box with side length L ($L=48\sigma$; volume $V=L^3$). The number density of the chain beads is $\rho_m=n\mathcal{N}/V=3.356\times10^{-2}\sigma^{-3}$ and the number density of counterions is $\rho_c=n_c/V=1.678\times10^{-2}$. The value of ρ_m is sufficiently low to correspond to a diluted polyelectrolyte solution. Note that the classical chain overlap density, $\rho^*\propto\mathcal{N}/(\frac{4}{3}\pi R_g^3)$, where R_g is the average radius of gyration of the electroneutral chain in a good solvent, is found to be $4.88\times10^{-2}\sigma^{-3}$ for the model under study. In addition, we simulated a diluted single-chain system consisting of a single 128-unit proteinlike chain plus 64 counterions enclosed in the same periodic cubic box. For this system we have 29-fold lower concentration of monomer units, $\rho_m=1.157\times10^{-3}\sigma^{-3}$.

The model systems were simulated at different temperatures varied in the range from $T=0.25$ to 3.0 (at $\rho_m=3.356\times10^{-2}\sigma^{-3}$) and from $T=0.25$ to 6.0 (at $\rho_m=1.157\times10^{-3}\sigma^{-3}$). Under conditions considered in the present study, these temperature ranges correspond to the Bjerrum length $l_B=e^2/4\pi\epsilon_0\epsilon_r k_B T$ ranged from 4 to 1/6 (in units of σ). Note that $l_B=7.1$ Å for water at room temperature. Since in our model, on average, every second monomer unit carries one elementary charge and the bond length is fixed at $b=\sigma$, the Manning parameter, $\xi_M=l_B/2b$, is varied from 1/12 to 2. The value of $\xi_M\geqslant1$ corresponds to a polyion which is strongly charged. The effective electrostatic screening is connected with the Debye–Hückel screening length κ^{-1} defined by $\kappa^2=(e^2N_A/\epsilon_0\epsilon_r k_B T)\Sigma_i q_i^2\rho_i$, where N_A is Avogadro's number, q_i is the charge on ion species i, and ρ_i is the bulk number density of ion species i. The variation of the temperature allows covering the wide range from low effective screening, with dominating electrostatic effects at high temperature, to high effective screening, with collapsed chains at low temperature. It should be stressed that a variation of the temperature in our simulations changes simultaneously both the strength of long-range electrostatic interactions and the intensity of short-range attractive hydrophobic interactions. This means that, similar to real experiments, a change of temperature influences all relevant quantities of the system in a rather complex manner.

For each temperature, the system was equilibrated for about 2×10^6 time–steps and then the production runs were performed. Typically, each production run was from 2×10^6 to 10^7 time–steps, depending on the temperature. The calculations are performed in standard reduced units, i.e., lengths are measured in units of σ; energy in units of ϵ; temperature,

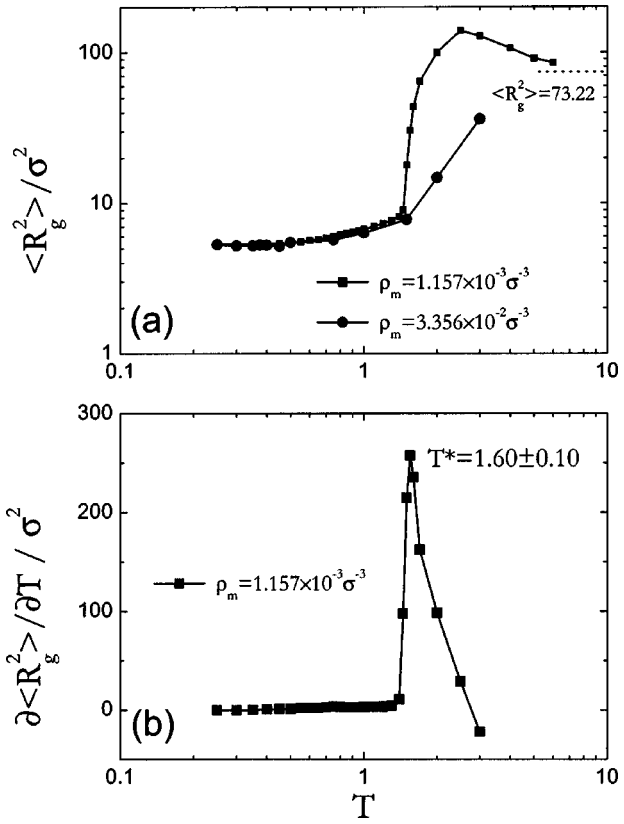

FIG. 2. (a) Temperature dependencies of $\langle R_g^2 \rangle$ for (■) the single-chain system (at $\rho_m = 1.157 \times 10^{-3} \sigma^{-3}$) and (●) the multichain system (at $\rho_m = 3.356 \times 10^{-2} \sigma^{-3}$). (b) The value of $\partial \langle R_g^2 \rangle / \partial T$ as a function of temperature, at $\rho_m = 1.157 \times 10^{-3} \sigma^{-3}$.

T, in units of ϵ/k_B; and time, t, in units of $\tau = \sigma \sqrt{m/\epsilon}$.

In the present study we focus mainly on equilibrium properties of the system. They include the mean-square radius of gyration of the chains, the time-averaged potential energies, the partial pair correlation functions and the structure factors, etc. In addition, we calculate the self-diffusion coefficient of counterions.

III. RESULTS AND DISCUSSION

A. Single-chain conformation and coil-to-globule transition

Although we are primarily interested in the intermolecular effects, we first characterize the behavior of a single charged $\mathcal{HP}$ copolymer that we use as a reference for comparison with multichain systems. In particular, we start our discussion by estimating the reference temperature at which the coil–globule transition takes place in a proteinlike polyion for the low-concentration limit. This problem is a first step towards a more precise understanding of collective properties.

Figure 2(a) shows the equilibrium averaged squared radius of gyration $\langle R_g^2 \rangle$ calculated for a single 128-unit charged proteinlike chain placed in a periodic box ($L = 48\sigma$) with $n_c = 64$ counterions as a function of temperature. For the system considered, the number density of chain beads is sufficiently low, $\rho_m = 1.157 \times 10^{-3} \sigma^{-3}$, so that we can treat the results as those corresponding to a dilute polyelectrolyte solution (as has been noted above, this monomer density is below the overlap density, ρ^*).

From the data shown in Fig. 2(a) it is seen that the squared radius of gyration fist increases with decreasing temperature starting from $T = 6.0$, reflecting the stretching of the chain (for the 128-unit charge-free chain in a good solvent, i.e., at $U_a = U_C = 0$ in Eq. (1), we find: $\langle R_g^2 \rangle = 73.22 \sigma^2$). At $T \approx 2.5$ ($l_B \approx 0.4\sigma$) the maximum value of $\langle R_g^2 \rangle$ is reached, and then the polyion starts to collapse, as expected. The nonmonotonic behavior of the chain size is due to the fact that the Bjerrum length increases with decreasing temperature. This increases the repulsion between like-charged monomer units, tending to elongate the chain as a whole. At the same time, the short-range attraction between hydrophobic units stabilizes compact conformations of the chain as temperature is decreased. In addition, the attraction of the counterions to the chain is also increased. The condensed counterions can approach the highly charged polyion very closely and form together with oppositely charged $\mathcal{P}$ units ion pairs, i.e., dipole-type configurations. This results in a screening the electrostatic repulsion between chain charges and leads to an additional electrostatic short-range attraction between the effective dipoles, tending to contract the chain. One can say that the polyion–counterions interaction effectively changes the solvent quality so that the solvent becomes poorer. At sufficiently high temperatures, the interaction between the polyions and counterions is weak so that the influence of the counterion-induced attraction on chain properties may be neglected (such a tendency is seen in Fig. 2(a) at $T > 6$).

The nonmonotonic dependence of the chain size on the strength of the electrostatic interaction was also observed in molecular-dynamics simulations of highly charged polyelectrolyte chains dissolved in a good solvent in the presence of counterions.[15,16] There are several theoretical approaches in which this effect is discussed.[34,35]

An apparent transition temperature, T^*, can be associated with the inflection point on the $\langle R_g^2(T) \rangle$ curve. Note that in order to estimate T^*, it is easier to use the radius of gyration than the specific heat. The derivative $\partial \langle R_g^2(T) \rangle / \partial T$ exhibits a pronounced peak, which signals a transition [see Fig. 2(b)]. After least-square fitting of the simulation data and subsequent differentiation, we find $T^* = 1.60 \pm 0.10$ for the energy parameters $\epsilon_{\mathcal{HH}}$, $\epsilon_{\mathcal{PP}}$, and $\epsilon_{\mathcal{HP}}$ used in the simulation. As has been noted, the values of $\epsilon_{\mathcal{HH}}$, $\epsilon_{\mathcal{PP}}$, and $\epsilon_{\mathcal{HP}}$ entering the attractive potential (3) were chosen equal to 2 in order to ensure the collapse of hydrophobic units into a dense core shielded by hydrophilic units from the solvent. At $T > T^*$, the polyion is in the expanded coil state and collapses when temperature becomes lower than T^*, indicating a dense globular structure of the chain. In the range $T < T^*$, a decrease in temperature results in a consistent decrease in $\langle R_g^2 \rangle$, suggesting that the size of the polyion decreases progressively toward more compact globular structures. Of course, the critical temperature T^* reported should not necessarily be taken as asymptotic ($\mathcal{N} \to \infty$); moreover, it depends upon the concentration of polymer in solution. Nevertheless, the estimated value of T^* should be relevant for the purposes of our study as a reference temperature.

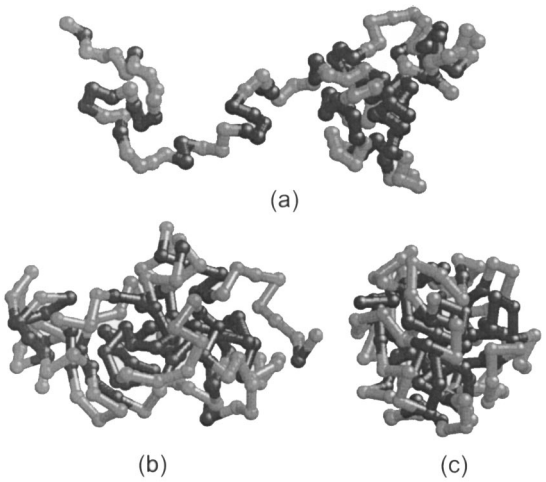

FIG. 3. Typical polyion conformations at (a) $T=3.0$, (b) $T=1.5$, and (c) $T=0.25$ for $\rho_m=3.356\times10^{-2}\sigma^{-3}$. The hydrophilic chain sections are presented as light spheres. Counterions are not shown.

Also, in Fig. 2(a) we compare the temperature dependence of $\langle R_g^2\rangle$, calculated for the multichain system (at $\rho_m=3.356\times10^{-2}\sigma^{-3}$), with that obtained for the single-chain system. As expected, higher system density causes stronger screening of electrostatic interactions, thus intrachain charge–charge repulsion is weaker and, respectively, the values of $\langle R_g^2\rangle$ are smaller, and their temperature dependence is less pronounced. However, the differences are well-pronounced only at sufficiently high temperatures. Indeed, for the strongly collapsed chains (at $T\lesssim1.4$) we have practically the same values of $\langle R_g^2\rangle$ for both systems.

In Fig. 3 we present three instantaneous pictures (snapshots) showing the typical polyion conformations obtained at different temperatures for $\rho_m=3.356\times10^{-2}\sigma^{-3}$. As seen in Fig. 3(a), in the high-temperature region ($T=3.0$), the chain has an extended conformation, caused by electrostatic repulsion, with small hydrophobic blobs. Such a conformation is well-known in the literature for polyelectrolytes under poor solvent conditions and can be considered as a string of hydrophobic blobs in the framework of the ''pearl-necklace'' model.[36] In poor solvents, for example, it is known that a necklace structure might be more favorable than the stretched (rodlike) conformation in certain regimes, due to the balance of short-range attractive and long-range repulsive forces.[34–37] In addition to pearl-necklace conformations there are also partially collapsed polyions. This suggests a plausible coexistence between these typical microstructures. As the temperature decreases, the formation of the globular conformation takes place. However, in the vicinity of the coil-to-globule transition temperature (at $T=1.5$), the charged globules, both in dilute and in more concentrated solution, have a friable structure [Fig. 3(b)]. At the lowest temperature considered here ($T=0.25$), we observe the formation of dense globules with a specific core-shell morphology characterized by the presence of a compact globular core consisting mainly of electroneutral hydrophobic $\mathcal{H}$ units and outer shell built up from charged hydrophilic $\mathcal{P}$ blocks [see Fig. 3(c)].

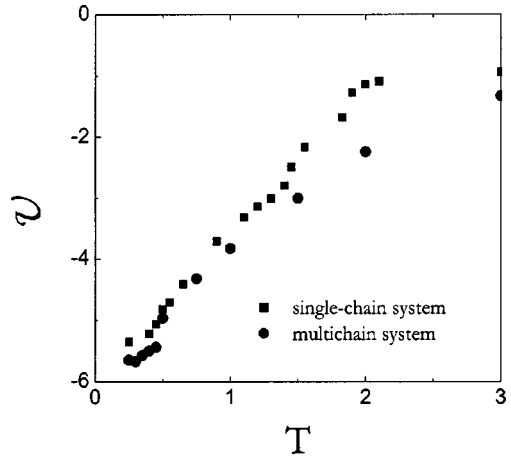

FIG. 4. Temperature dependencies of the reduced potential energy $\mathcal{V}$ for (■) the single-chain system ($\rho_m=1.157\times10^{-3}\sigma^{-3}$) and (●) the multichain system ($\rho_m=3.356\times10^{-2}\sigma^{-3}$).

B. Thermodynamic properties

Figure 4 shows the reduced potential energy per particle, $\mathcal{V}=U/\epsilon N$ (where U is the total potential energy calculated at each time–step and averaged over the full simulation) as a function of temperature for the single-chain and multichain systems. For both systems under conditions considered in our simulations, the reduced energy per particle $\mathcal{V}$ is strongly negative, corresponding to a poor solvent condition, and becomes more negative as the temperature is decreased. In the case of the multichain system, the $\mathcal{V}$ curve is slightly below the one for the single-chain system.

The temperature dependence of the reduced Coulomb energy per particle $\mathcal{V}_C$ is of particular interest. As seen in Fig. 5, where we present the results for the single-chain and multichain systems, the dependence of $\mathcal{V}_C$ on T is a complex function. With decreasing T, the Coulomb energy $\mathcal{V}_C$ initially increases, achieves a maximum value at $T\approx1.5$, and then begins to drop, showing a nonmonotonic behavior in the low-temperature region for the multichain system. What is relevant here is the fact that for all the temperatures considered in the present study the Coulomb energy remains posi-

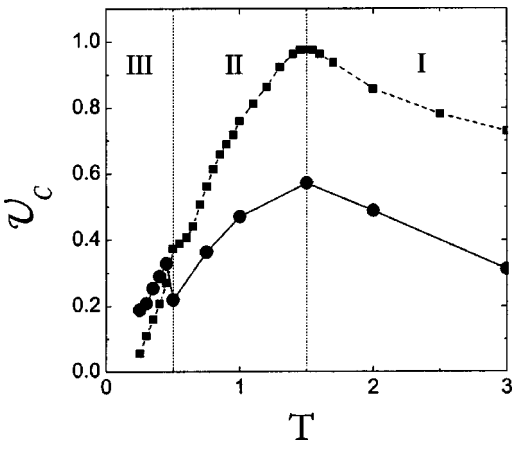

FIG. 5. Total reduced Coulomb energy $\mathcal{V}_C$ as a function of temperature for (■) the single-chain system ($\rho_m=1.157\times10^{-3}\sigma^{-3}$) and (●) the multichain system ($\rho_m=3.356\times10^{-2}\sigma^{-3}$).

tive. Therefore, the negative values of $\mathcal{V}$ seen in Fig. 4 are due to strong short-range attractive interactions between chain beads.

In order to explain the behavior of $\mathcal{V}_C$ in more detail, it is instructive to present the total Coulomb energy of the system as the sum of the following three terms:

$$\mathcal{V}_C = \mathcal{V}_{mm} + \mathcal{V}_{cc} + \mathcal{V}_{mc}, \tag{7}$$

where $\mathcal{V}_{mm}$ is the energy of intra- and interchain monomer–monomer interactions, $\mathcal{V}_{cc}$ is the energy of counterion–counterion interactions, and $\mathcal{V}_{mc}$ denotes the (negative) energy of polyion–counterion cross interactions.

An increase in $\mathcal{V}_C$ observed with decreasing temperature in the region $1.5 < T < 3.0$ can be simply explained by a decrease in chain extension [see also Fig. 2(a)]. In this temperature region, the behavior of each individual polyion is mainly governed by the nonionic short-range attraction between chain beads, resulting in the formation of more compact chain conformations [see Figs. 2(a) and 3(a)]. However, for this high-temperature regime (which we will call below *regime* I) we always observe expanded coil-like conformations of the polyions. It is clear that, as the chain conformation becomes more compact, the distances between charges on each individual chain decrease, causing an increase in the $\mathcal{V}_{mm}$ term. On the other hand, under these conditions, counterions are distributed in the system more or less uniformly and the $\mathcal{V}_{cc}$ and $\mathcal{V}_{mc}$ terms change weakly with temperature. One can say that the regime I corresponds to a typical polyelectrolyte solution in which swollen chains are well-separated [see Fig. 6(a), where a snapshot of the system is presented]. In this case, the electrostatic attraction is not strong enough to keep counterions adjacent to the polyion, and they are spread throughout the solution. Nevertheless, counterions are not distributed uniformly but are more likely to be found near the oppositely charged polyions. In some cases counterions condense on charged macromolecules reducing the effective charge of polyions.

When the formation of globular conformations is practically completed, we find ourselves in a new *regime* II, $0.4 \lesssim T \lesssim 1.5$. In this regime, the further decrease in temperature does not lead to a significant redistribution in the intrachain distances between charged sites, thus making the $\mathcal{V}_{mm}$ term almost constant. On the other hand, at $T < 1.5$, a well-pronounced redistribution of counterions in the system begins, reflecting the change in the degree of counterion condensation. In this case, the $\mathcal{V}_{mc}$ term begins to show strong temperature dependence. Obviously, the condensation of free counterions on the oppositely charged surface of globules should result in a strong decrease in $\mathcal{V}_{mc}$. The snapshot of the corresponding configuration [see Fig. 6(b)] shows that in the regime II (at $0.4 \lesssim T \lesssim 1.5$) no aggregation of individual globules is observed for the multichain system, implying that in this case the system lies in the stable one-phase region. It is seen that in the dilute solution of collapsed polyelectrolytes some counterions are still distributed far from polyions while others are located in their vicinity and form surrounding clouds in the regions close to the surface of globules. It should be noted that the reduced internal pressure, pV/Nk_BT, calculated for the multichain system from the virial equation and averaged over the duration of the simulation, becomes negative at $T \lesssim 1.5$ (not shown).

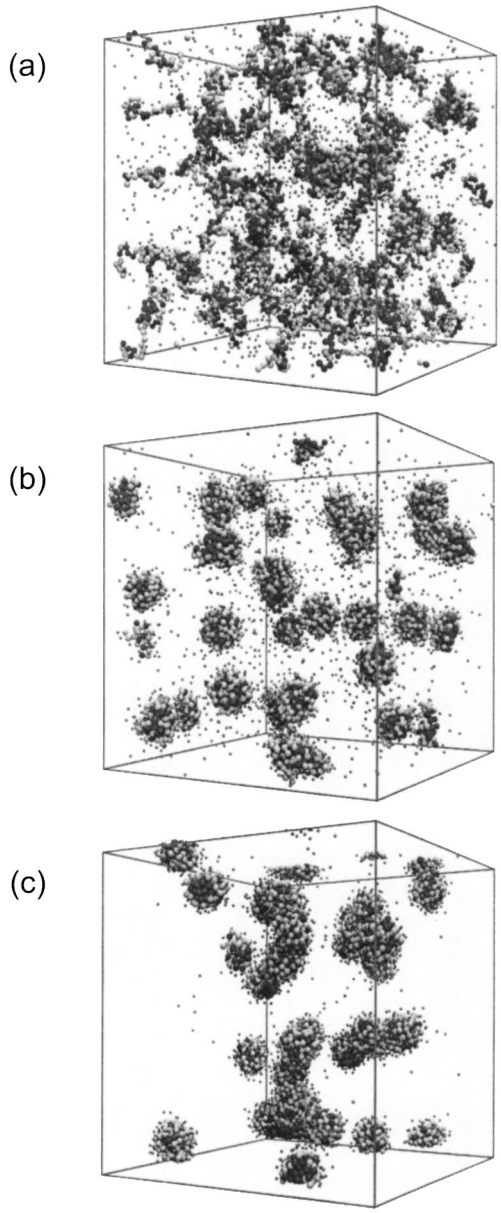

FIG. 6. Snapshots of the whole simulations box at (a) $T=3.0$, (b) $T=1.0$, and (c) $T=0.25$ for $\rho_m = 3.356 \times 10^{-2}\sigma^{-3}$. The light spheres depict charged polymeric units. The counterions are presented as small spheres.

In the regimes I and II, the total electrostatic energy per particle calculated for the multichain system is distinctly lower than for the single-chain system. This is due to stronger screening of electrostatic interactions at higher system density, the fact mentioned above.

When the system temperature is further decreased, most of the counterions are in a ''bound counterion'' state, i.e., they are strongly associated with the oppositely charged chain sites. In other words, counterions try to associate with negatively charged $\mathcal{P}$ units more closely and form bound ionic states (i.e., ion pairs). In addition to counterion condensation, we observe for this low-temperature regime the aggregation of isolated globules in the multichain system. From very long MD simulations carried out at equilibrium we con-

clude that, when the temperature becomes progressively lower, the polyion globules can stick together, forming pairs, triplets and (seldom) multiplets and nearly all counterions are associated with aggregated macroions. This conclusion can be drawn from the analysis of snapshot pictures [see, e.g., Fig. 6(c)] and pair correlation functions discussed below. Naturally, this process is accompanied by a further decrease in the total potential energy of the system due to an increase in the number of interchain short-range attractive contacts (see Fig. 4). At the same time, the separation between negatively charged surfaces of the globules shortens, causing an increase in the electrostatic energy of monomer–monomer interaction $\mathcal{V}_{mm}$. As a result, the total Coulomb energy shows a jumplike rise observed for the multichain system at $T \approx 0.4$ (Fig. 5). We can identify all these features as an evidence of the transition of the multichain system to a new low-temperature regime (*regime* III). Of course, for the single-chain system, there is no contact-induced jump in $\mathcal{V}_C$ because in this case the intramolecular term $\mathcal{V}_{mm}$ of an isolated globule, making no contacts with others, changes weakly and, therefore, the Coulomb energy changes monotonically with temperature. With further decreasing temperature, one observes an almost total counterion condensation (as we will see below, this is also important for the understanding of transport phenomena). Besides, some redistribution of the charged chain sections located mainly at the globular surfaces takes place. It is clear that these factors should anyhow lead to some decrease in the value of $\mathcal{V}_C$, the result indeed observed in Fig. 5 for both systems. Naturally, without repulsive intermolecular contribution to $\mathcal{V}_{mm}$, the value of $\mathcal{V}_C$ found for the single-chain system becomes lower as compared to that observed for the multichain system.

Thus, from the analysis of the temperature behavior of the Coulomb energy, we suggest the existence of three different temperature regimes in poor solutions of flexible proteinlike polyelectrolytes. Similar trends can be seen in other properties, which will be discussed in this paper.

The transitions between the temperature regimes are found to be thermodynamically reversible. As an example, let us consider the transitions from the intermediate-temperature regime II (the globular state, $T=1.0$) to the low-temperature regime III (the globular state, $T=0.4$), then back to the regime II ($T=1.0$), next to the high-temperature regime I (the coil-like state, $T=3.0$), and then back to the regime II ($T=1.0$). Figure 7 shows the corresponding time evolutions of the squared radius of gyration and the reduced electrostatic energy per particle, $\mathcal{V}_C$, for the multichain system. As can be seen, the temperature transitions between the globular states and the coil-like state are thermodynamically reversible, thus indicating that the system under study does not get trapped in metastable states.

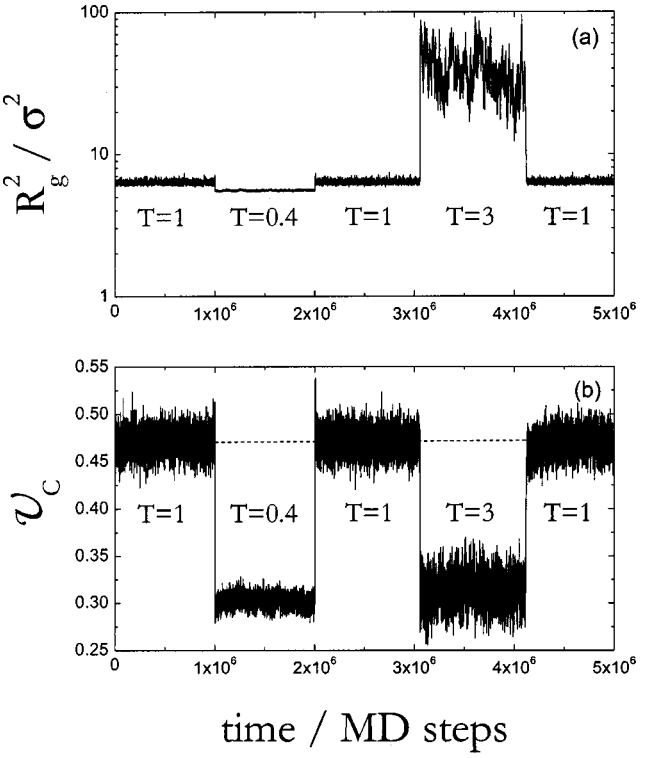

FIG. 7. The time evolutions of (a) the squared radius of gyration and (b) the reduced electrostatic energy $\mathcal{V}_C$ for the multichain system.

C. Counterion condensation

From the Manning theory of counterion condensation,[41] it is known that there exists a Bjerrum length, l_B^* (or the corresponding temperature, T_c) separating two different regimes in the behavior of a polyelectrolyte solution. For l_B below this critical value l_B^*, the counterions would simply repel each other due to a reduction of the Coulomb interaction. On the other hand, above this value, the effective potential for the counterions is attractive and the counterions condense on the polyion. For a hard-core system in the limit of zero concentration and infinite polyion length, the Manning theory predicts $l_B^* = \sigma$; that is, $T_c = 1$.

In order to estimate the critical temperature of counterion condensation, T_c, we can use the radius R^* as a measure for the reduced charge of the chain. This quantity is defined as the average radius of a sphere around a charged monomer unit that contains one counterion. Although we do not formulate any rigorous criterion as to which counterions are close enough to the polyion to be called ''bound,'' we should consider the value of R^* as a reasonable indicating parameter.

To describe the local environment formed in the vicinity of chain beads, we calculated the monomer–counterion pair correlation functions $g_{mc}(r)$, which defines the probability of finding a counterion within a spherical shell of volume $4\pi r^2 dr$ at a distance r from a given monomer unit, relative to that expected from their random distribution in the system. In addition, the corresponding running integration numbers, $n_c(r)$, were found. They are defined as

$$n_c(r) = 4\pi\rho_c \int_0^r g_{mc}(x) x^2 dx, \tag{8}$$

where ρ_c is the number density of the counterions. The value of $n_c(r)$ is the average number of counterions around a given monomer unit at a distance r.

Using the monomer–counterion pair correlation function the value of R^* can be calculated from the equation

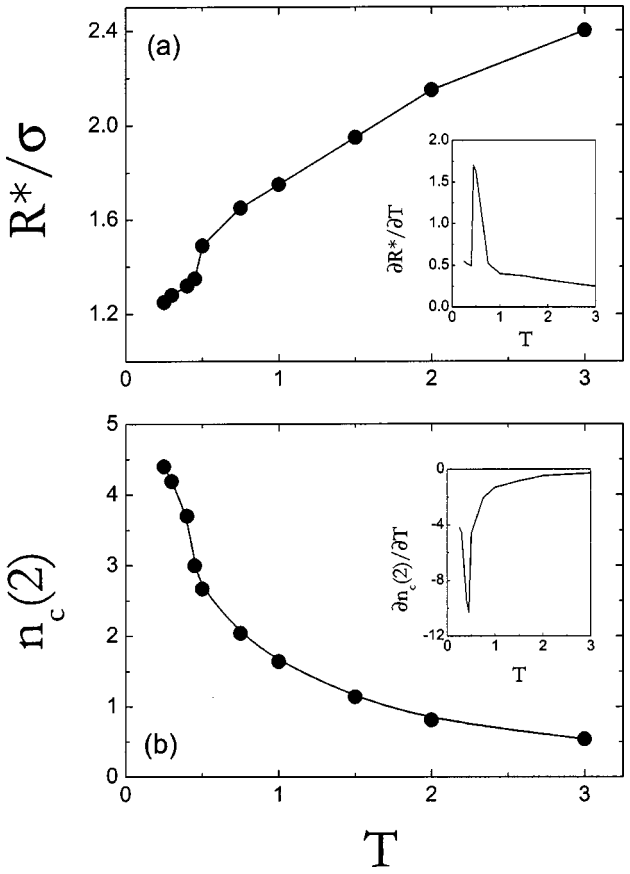

FIG. 8. (a) Recharged radius R^* as a function of temperature for the multichain system. (b) The average number of counterions $n_c(2)$ within a distance $r=2$ from a given chain site for various temperatures, at $\rho_m=3.356\times10^{-2}\sigma^{-3}$.

$$4\pi\rho_c\int_0^{R^*} g_{mc}(r)r^2\,dr=1. \tag{9}$$

Figure 8(a) presents R^* as a function of temperature for the multichain system. This figure shows that R^* decreases with decreasing temperature and approaches $R^*=1.2\sigma$ as the temperature drops to 0.25. At zero temperature, R^* should be equal to 1. The derivative $\partial R^*/\partial T$ has a rather sharp peak in the neighborhood of $T\approx0.5$ ($l_B\approx2\sigma$). This temperature can be considered as the critical temperature of counterion condensation, T_c.

Figure 8(b) depicts the average number of counterions $n_c(2)$ within a distance $r=2\sigma$ from a given chain site for various temperatures. In the limiting case of the most dense hexagonal package, each bead of a freely jointed chain with bond lengths fixed at $b=\sigma$ can be surrounded by ≈10 nonbonded neighbors. For a bead located at an infinite interface, this number is reduced to $n_{\max}\approx5$. From the data presented in Fig. 8(b) we can find that at $T=0.25$ the ratio $n_c(2)/n_{\max}$ is about 0.9, thus indicating almost complete counterion condensation on the surface of globules. Regarding this result, it should be taken into account that at low temperature the counterion clouds surrounding the polymer globules contact with each other [see, e.g., Fig. 6(c)]. Therefore, the counterion clouds from different polyions can contribute to $n_c(2)$. The derivative $\partial n_c(2)/\partial T$ shows a sharp peak in the vicinity of $T\approx0.5$. This value is practically the same as the critical temperature of counterion condensation estimated from Eq. (9).

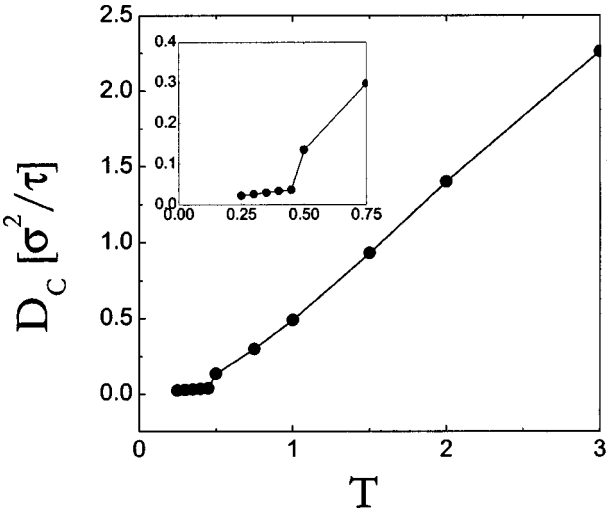

FIG. 9. Self-diffusion coefficient of the counterions D_C (in units of σ^2/τ) as a function of temperature at $\rho_m=3.356\times10^{-2}\sigma^{-3}$.

As an alternative criterion of counterion condensation, we can use the cross correlation between counterions and polymer chains. It is clear that the motions of the bound counterions are strongly correlated to the polyions. Since the polyions are more massive than the counterions, they would restrict the motion of the bound counterions and their mobility can be radically different from the mobility of free counterions. As a result, the self-diffusion coefficient of the counterions, D_C, would exhibit a substantial reduction, when the degree of counterion condensation is sufficiently high. Of course, in addition to the formation of ion pairs, also larger groups of counterions could be formed near the surface of globules.

The self-diffusion coefficient of an individual counterion can be calculated from its mean-square displacement (MSD) using the Einstein relation[28]

$$D_C=\frac{1}{6t}\langle|\mathbf{r}(t)-\mathbf{r}(0)|^2\rangle_{t\to\infty}, \tag{10}$$

where the angular brackets denote an ensemble average or, equivalently, an average over different time origins $t=0$ and $\mathbf{r}(t)$ is the position vector of a counterion after the time interval t has elapsed. For the self-diffusion case, the ensemble average is performed over all counterions as well as over all time origins since $\mathbf{r}(t)$ is a single particle property. The procedure used here for calculating the appropriate time averages of the transport coefficients involved the method of running averages.[28] One should note that for some of the runs (for the lowest temperatures), the MSDs were too noisy to establish unambiguously where the Einstein behavior (10) has been reached.

The counterion self-diffusion coefficients are presented in Fig. 9 for various temperatures. As expected, the value of D_C decreases with decreasing temperature, indicating an increasing degree of counterion condensation. For the highest temperatures studied (in the range $T\gtrsim1$), D_C is apparently a

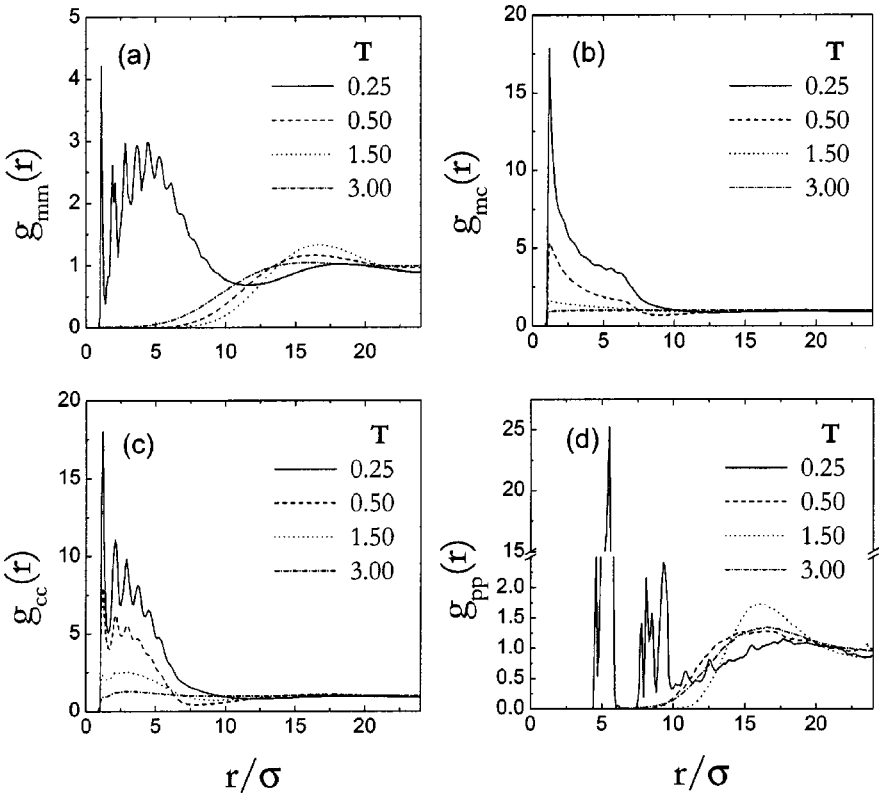

FIG. 10. Pair correlation functions (a) $g_{mm}(r)$, (b) $g_{mc}(r)$, (c) $g_{cc}(r)$, and (d) $g_{pp}(r)$ for the system of charged proteinlike chains at different temperatures at $\rho_m = 3.356 \times 10^{-2}\sigma^{-3}$.

linear function of temperature. As the temperature decreases below $T \approx 1$, the temperature dependence of D_C deviates from linearity. At $T \lesssim 0.5$, we observe in Fig. 9 that D_C drops sharply, indicating the onset of counterion condensation.

From the data presented above we can conclude that the different criteria of counterion condensation used here predict practically the same critical temperature of counterion condensation, T_c. Note that this value is considerably smaller as compared to that predicted by the Manning theory. The difference can be due to the fact that in our system counterions condense on the surface of globules which have nearly spherical shape.

D. Correlation functions

The structure of the solution was characterized by pair-correlation functions (PCFs) and structure factors, providing an information on charge distribution and order in the system.

The local structure of the system was examined via the following pair-correlation functions: The monomer–monomer PCF, $g_{mm}(r)$; the counterion–counterion PCF, $g_{cc}(r)$; the monomer–counterion PCF, $g_{mc}(r)$; and the polyion–polyion PCF, $g_{pp}(r)$. Note that $g_{pp}(r)$ describes the spatial distribution of centers-of-mass of polyion chains. All these functions are shown in Fig. 10 for four different temperatures corresponding to the temperature regimes I, II, and III introduced above. Although the averaging was performed over very long runs, there is still substantial statistical noise in the simulation results, especially at low temperatures. Taking into account this fact, we will focus only on the main features of the PCFs.

In particular, we have found that all PCFs change their character gradually from high to lower temperature when we consider the transition from the temperature regime I to the regime II. The transition to the low-temperature regime III is accompanied by dramatic changes in the monomer–monomer and polyion–polyion PCFs [see examples shown in Figs. 10(a) and 10(d)], while the functions $g_{cc}(r)$ and $g_{mc}(r)$ do not display such dramatic changes in this case.

From the analysis of the monomer–monomer and polyion–polyion PCFs, we can conclude that there is a correlation hole for distances smaller than roughly 5σ at temperatures corresponding to the regime I when polyions are in coil-like state. At lower temperatures corresponding to the regime II, the correlation hole becomes wider and moves to longer distances ($\approx 10\sigma$). This fact indicates that polyions, being in globular state, cannot come closer together than the distance $\approx 10\sigma$. It should be emphasized that for the globular state this distance is much larger than mean size of the globule [see Fig. 2(a)]. Thus, we can draw the following conclusion: Under conditions corresponding to the second temperature regime, when the chains are in a globular state, there is a sufficiently strong repulsive interaction pushing globules away from each other and thus preventing their aggregation into a large cluster. This conclusion is supported by a visual inspection of a large number of snapshots similar to those shown in Fig. 6(b). On the other hand, from Figs. 10(a) and 10(d) we can see that for the regimes I and II there is a weak peak in the intermolecular pair correlation functions $g_{mm}(r)$ and $g_{pp}(r)$ at large separations. Since the potential of mean force is defined as $-k_B T \ln[g(r)]$ an effective attraction emerges in the potential of mean force at separations where this peak exists. As the temperature is lowered the peak first

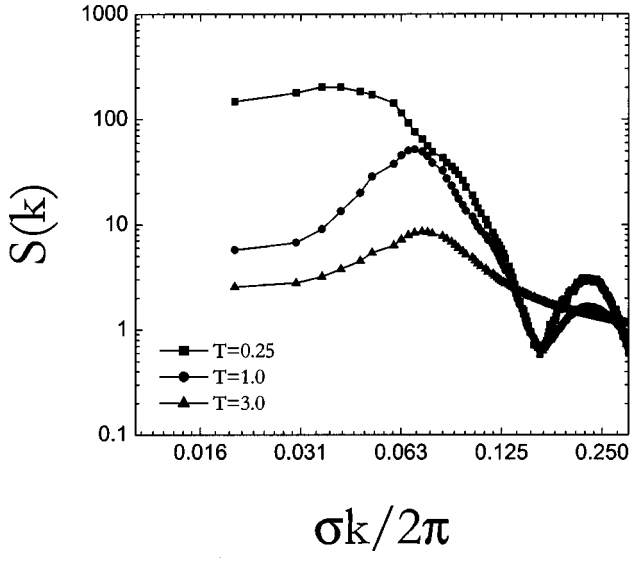

FIG. 11. Total static structure factor $S(k)$ for the system of charged protein-like chains at different temperatures at $\rho_m = 3.356 \times 10^{-2} \sigma^{-3}$. The value of $S(k) = 1$ corresponds to a system with uncorrelated particles.

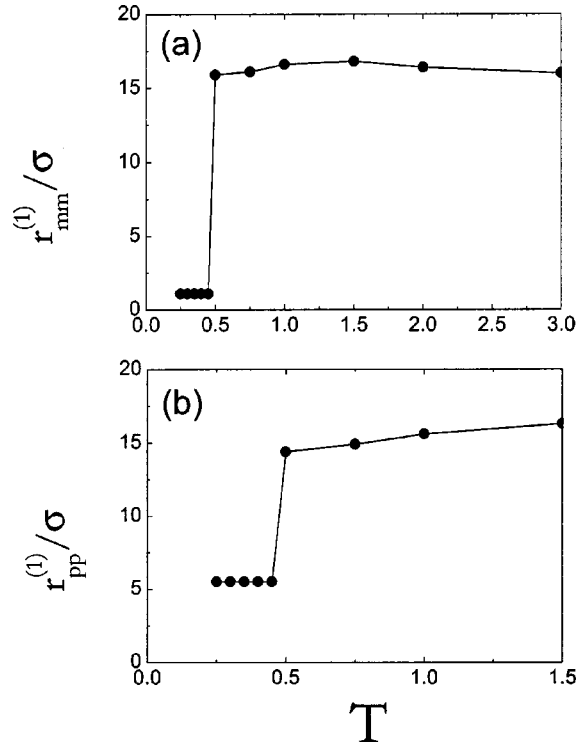

FIG. 12. Temperature dependencies of the characteristic distances $r_{mm}^{(1)}$ and $r_{pp}^{(1)}$ corresponding to the monomer–monomer and polyion–polyion correlation functions at $\rho_m = 3.356 \times 10^{-2} \sigma^{-3}$.

becomes stronger (at $T = 1.5$) and then decreases at sufficiently low temperatures. Also, from Fig. 10(c) it is seen that an almost imperceptible peak in $g_{cc}(r)$ appears at $T = 3$ on a short length scale of the order of σ.

Further evidence for the formation of the stable nonaggregated structure of globules similar to strongly interacting charge-stabilized suspensions or charged microgels can be gained from the analysis of the static structure factor, $S(k)$, which characterizes the spatial organization of the system as a whole. We have calculated the static structure factor of the whole simulation box that reflects the arrangement of the chains and counterions in space. The function $S(k)$ is presented in Fig. 11 for three temperatures. Although there are technical problems connected with the calculation of $S(k)$, due to the fact that it is strongly influenced by finite size effects (especially at small wave numbers **k**), from Fig. 11 we can definitely see that the function $S(k)$ has a ''small angle'' peak for the temperatures corresponding to the regimes I and II. The main maximum of $S(k)$ implies that the system is spatially inhomogeneous at the intermediate scale related to the average interchain distance. The scattering intensity increases with decreasing temperature. Clearly, the position of the main peak, k^*, is determined by the interchain correlations at long distances and connected with the correlation holes seen in Figs. 10(a) and 10(d) for the monomer–monomer and chain–chain PCFs. Indeed, the characteristic wave number k^* determines the average distance r^*, given by the Bragg condition $r^* = 2\pi/k^*$, between scattering objects; e.g., at $T = 1.0$ we find $r^* \approx 15\sigma$, the value which is close to the size of the correlation hole. If we assume a uniform distribution of nonaggregating globules in the simulation box, we obtain the following estimation: $r^* = L/\sqrt[3]{n} = 15.6\sigma$. On the other hand, for uniformly distributed dimers formed by the aggregating globules this distance would distinctly increase ($r^* = L/\sqrt[3]{n/2} = 19.7\sigma$) and would become even longer for trimers and larger aggregates. All these findings indicate that in the temperature regime II we deal with a system of single-chain nonaggregating globules, which repel each other because they still have a sufficiently high net charge. Indeed, as has been shown in the previous subsections, there is some fraction of free (noncondensed) counterions even at the lowest temperatures studied in the present work. A similar conclusion has been drawn by Kremer and co-workers.[23,24] In particular, they observed no agglomeration or phase separation for a system containing charged globules.

When the temperature is further decreased (i.e., the Bjerrum length is increased), we observe dramatic changes in the monomer–monomer and chain–chain PCFs, as has been noted above. Naturally, the structure factor of the system also reflects these features. At the temperature slightly below 0.5 (for $l_B \gtrsim 2\sigma$), the main maximum of $g_{mm}(r)$ and $g_{pp}(r)$ sharply shifts towards shorter distances, where these functions also show multiple satellite peaks due to the formation of ''fine structure.'' In Fig. 12 we present the positions of these maxima, $r_{mm}^{(1)}$ and $r_{pp}^{(1)}$, plotted versus temperature. One can see that the values of $r_{mm}^{(1)}$ and $r_{pp}^{(1)}$ show a jumplike decrease at $T < 0.5$ and then remain eventually constant at all the temperatures corresponding to the region III defined above. Notice that the shortest polyion–polyion distance $r_{pp}^{(1)}$ is still slightly larger than the characteristic size of the globule at the lowest temperature considered here, indicating a preservation of a counterion monolayer in the gap between the collapsed macroions (for example, at $T = 0.25$, one has: $\langle R_g^2 \rangle = 5.35 \pm 0.05\sigma^2$ and $\sqrt{\langle R_g^2 \rangle} = 2.31\sigma$). This means that neighboring globules, in principle, can touch each other or even can stick together, but they cannot interpenetrate at the

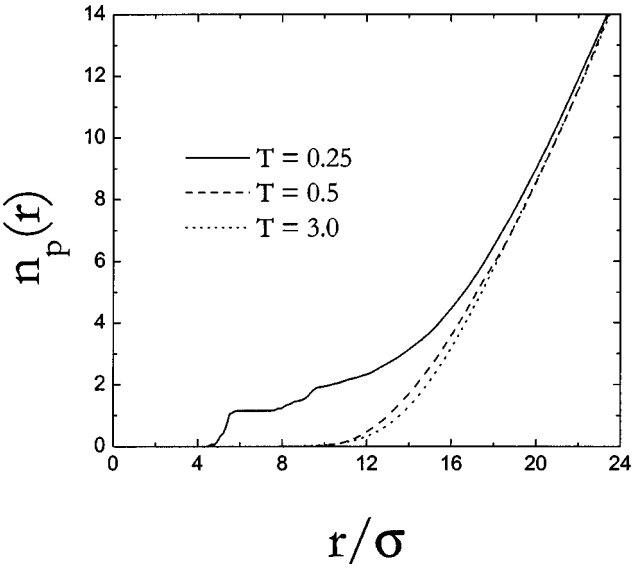

FIG. 13. Running coordination number, $n_p(r)=4\pi(n/L^3)\int_0^r g_{pp}(x)x^2dx$, for $T=0.25$, 0.5, and 3.0, at $\rho_m=3.356\times10^{-2}\sigma^{-3}$.

concentrations of polyelectrolyte solutions considered here. The snapshot presented in Fig. 6(c) confirms such conclusion.

By integrating the polymer center-of-mass correlation function $g_{pp}(r)$, one can estimate the average number of polyions around a given polyion at a distance r. The corresponding running coordination number, $n_p(r)$, is shown in Fig. 13 for $T=0.25$, 0.5, and 3.0 as a function of r. It is seen that the trends in the running coordination numbers observed for different temperatures are quite different. At $T=0.25$, there is a plateau in $n_p(r)$ in the short-distance region, the feature indicating the formation of a well-defined first coordination sphere. From these data we find that each polyion in the globular state has ~1.2 neighbors on the average within a distance of 7σ around it. On the other hand, $n_p(r)$ is a monotonically increasing function for $T\geqslant0.5$.

The structure factor also displays dramatic changes in the low-temperature region. The small-angle peak practically vanishes and the $S(k)$ curve transforms to that being similar to a macrophase-separating system, when $k^*\to0$ (Fig. 11). Such behavior reflects a large-scale instability of the system. In principle, these trends should be observed in neutron and light scattering experiments. The accuracy of our calculations precludes a reliable determination of how the position of the main peak in $S(k)$ scales with temperature.

Thus, our results show that there is an effective attraction between charged proteinlike globules when the temperature is sufficiently low (the regime III). However, the globules do not interpenetrate significantly under these conditions. A visual analysis of snapshot pictures [see Fig. 6(c)] gives some arguments suggesting the formation of specific elongated (chainlike) aggregates built up from individual stable globules surrounded by partly condensed counterions. As it follows from the data discussed in the previous subsection, such chainlike morphology can be due to repulsion between noncompensated charges on single collapsed chains. The counterions bound on the surface of nearly spherical globules play the role of the specific ''glue,'' sticking the globules together and, at the same time, preventing their aggregation into a single large aggregate (at least, for the conditions and copolymer primary sequences studied here). A visual examination of the instant configurations shows that most of the globules form pairs or triplets (see also Fig. 13).

Returning to the analysis of PCFs, we note that the first maximum of the counterion–counterion and polyion–counterion PCFs becomes more pronounced with decreasing temperature. The temperature changes observed for $g_{mc}(r)$ show that the local density of the counterions around the polyelectrolyte chains grows, clearly demonstrating the accumulation of the counterions near the macroions. At the lowest temperature considered here, the contact value of $g_{mc}(r)$ is ~17, meaning that the counterion number density at the macroion surface is ≈17 times as large as the average counterion density for the bulk solution. The origin of a multiple-peak pattern observed for the counterion–counterion PCF in Fig. 10(c) for the low-temperature regime can be interpreted as the formation of a partially ordered structure in the distribution of the counterions condensed on the globular surfaces. Such behavior reflects the combined effect of the electrostatic repulsion among the condensed counterions themselves and their attraction to the oppositely charged polyions. The slow decay of $g_{cc}(r)$ to 1 with increasing r reflects the correlation of counterions associated with the aggregated polyions.

The total structure factor $S(k)$ can be decomposed into the following two partial structure factors:

$$S_\alpha(k)=\frac{1}{N_\alpha}\sum_{i=1}^{N_\alpha}\sum_{j=1}^{N_\alpha}\langle\exp(i\mathbf{k}\cdot\mathbf{r}_{ij})\rangle, \tag{11}$$

where the index α corresponds to counterions ($\alpha=c$) or *charged* ($\mathcal{P}$) sites on the polyions ($\alpha=m$) and N_α is the number of these particles ($N_\alpha=n_c=\frac{1}{2}n\mathcal{N}$). The normalization for $S_\alpha(k)$ is $S_\alpha(0)=k_BT\rho_\alpha\chi_T$, where ρ_α is the partial density and χ_T denotes the compressibility. In Fig. 14 we plot the $S_m(k)$ and $S_c(k)$ functions for various temperatures and $\rho_m=3.356\times10^{-2}\sigma^{-3}$. In the high-temperature regime, there is a broad peak in $S_m(k)$ which narrows and moves very slowly to lower wave vectors as the temperature is decreased. At $T\gtrsim2$, the magnitude of counterion–counterion correlations appears to be relatively insensitive to T and negligibly small as compared to that observed for monomer–monomer correlations. It is clear that the source of a peak in $S_c(k)$ is the counterions clustering around the polyions. For sufficiently low temperatures, we find prominent peaks in the counterion–counterion partial structure factors at roughly the same wave numbers as the peaks in $S_m(k)$. In is easy to understand that this is a manifestation of the fact that the counterion correlations near the charged chain sites is very high, i.e., the counterion distribution is strongly correlated with that of the polyions.

Thus, our calculation of correlation functions confirms the existence of three different temperature regimes, which are characterized by different spatial organization of charged proteinlike copolymers and their conformational behavior under poor solvent conditions. In particular, at intermediate

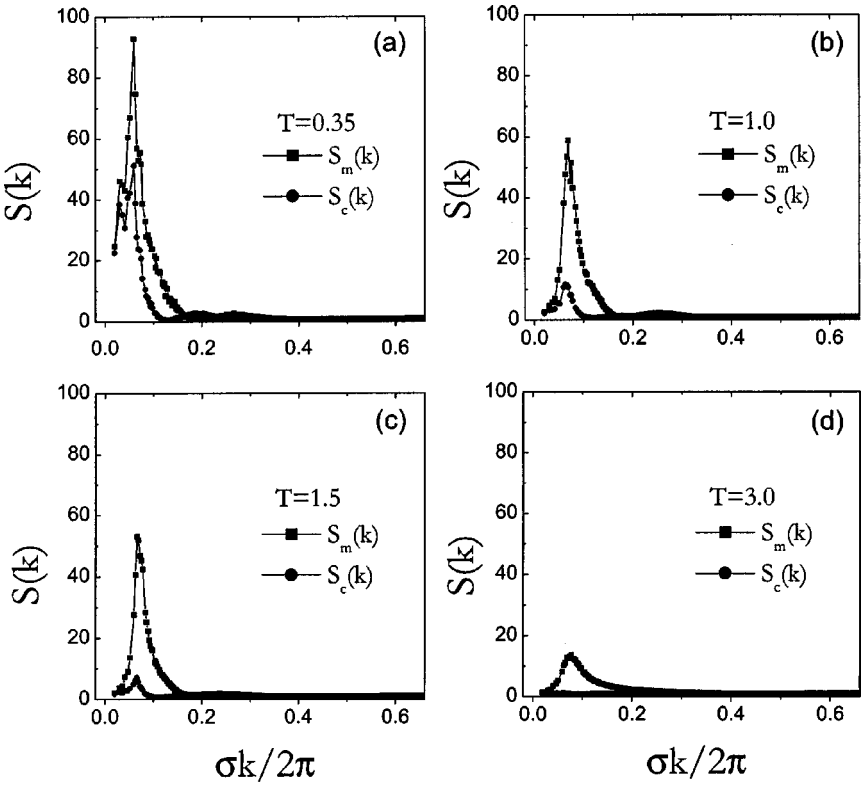

FIG. 14. Partial structure factors $S_m(k)$ and $S_c(k)$ for various temperatures and $\rho_m = 3.356 \times 10^{-2}\sigma^{-3}$.

temperatures (regime II) we observe a stable array of nonaggregating polymer globules which are well separated from each other. The transition between this regime and the high-temperature regime I looks like a smooth crossover. As the temperature becomes lower, we observe a sharp transition from the regime II to the regime III, giving rise to the formation of ''mesoglobules,'' i.e., supramolecular aggregates composed of more than one chains and having an elongated morphology. From the data shown in Figs. 4 and 5 we can conclude that short-range (nonelectrostatic) attractive interactions between polyion chains are the main driving force for this behavior. Also, it seems that the additional origin of attractive forces between like-charged globules is the formation of ion pairs on the surface of the globules. A similar effect has been observed in the MD simulations of Winkler *et al.*,[16] who studied the conformational properties of single strongly charged polyelectrolyte homopolymers of various lengths in the presence of counterions. It was found that, above the critical value for Manning condensation, counterions condense on the chain and ion pairs are formed. The resulting attractive interaction (thermally averaged monopole–dipole and dipole–dipole interactions decaying as r^{-6}) can lead to a collapse of the whole chain into a very compact structure. It should be stressed that it is exactly this behavior, which is responsible for the collapse of polymer chains and gels after extra ionization.[38–40] The presence of attractive intra- and interchain interactions has been also observed by Chu and Mak[17] in their computer simulation of flexible polyelectrolyte chains at nonzero concentrations with explicit counterions and unscreened Coulombic potential. It was shown that interchain attraction can arise from the charge fluctuations along the backbone of the chains as condensed counterions come on and off the chains. Earlier, Ray and Manning[42] suggested that two like-charged objects (e.g., rigid rods) can share counterions in such a way to form what is analogous to a covalent bond. A similar picture is observed in our simulations for the low-temperature regime when two or more dense globules stick together due to the counterion condensation on the globular surfaces. Note that the effective electrostatic attraction is evident only for systems having very large Bjerrum lengths (or at sufficiently low temperature), when one can overcome the Coulombic repulsion.

E. Stabilization of globules versus aggregation

A deeper insight into possible structures formed by two charged globules may help to understand general processes of the interactions between globular polyelectrolytes in dilute solutions, where the behavior of the solution is determined by the aggregates of two or only a few chains. To this end, we performed the following computer experiment. We started our simulation with two well-separated proteinlike globules ($\mathcal{N}=128$) enclosed in a periodic cubic box (side length $L=48\sigma$) containing also the corresponding number of counterions to ensure the condition of electroneutrality. During the simulations, we set $T=1$, the temperature at which the 128-unit chains are in compact globular state. Turning off the electrostatic interaction, we allowed the globules to attract each other due to strong hydrophobic interactions so that they formed a single biglobular complex. This complex was relaxed for a long time, resulting in compact globular agglomerate (''droplet'') with nearly spherical shape. After this initial stage, we turned on the Coulomb interaction and relaxed the system for 10^3 MD time–steps. Then we monitored the evolution of the system. The kinetic energy (temperature) was essentially constant since the system was

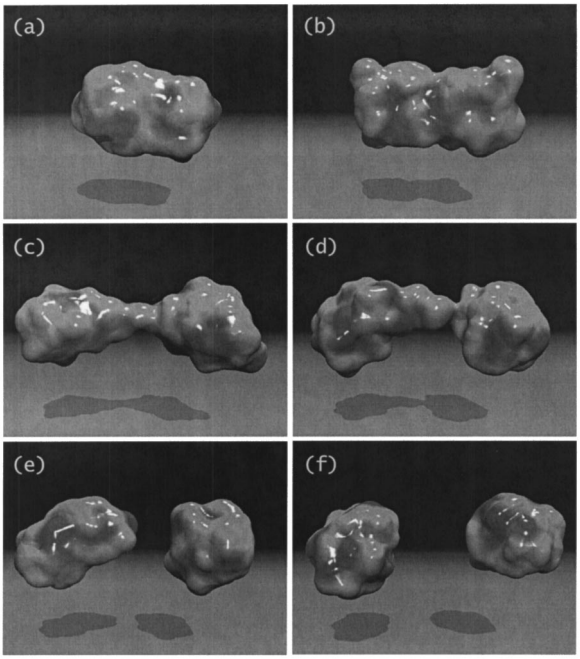

FIG. 15. Sequence of images, which illustrates the evolution of the aggregate of two charged macromolecules after switching on the Coulomb interaction at: (a) $t=0$, (b) $t=5\tau$, (c) $t=100\tau$, (d) $t=110\tau$, (e) $t=120\tau$, and (f) $t=170\tau$.

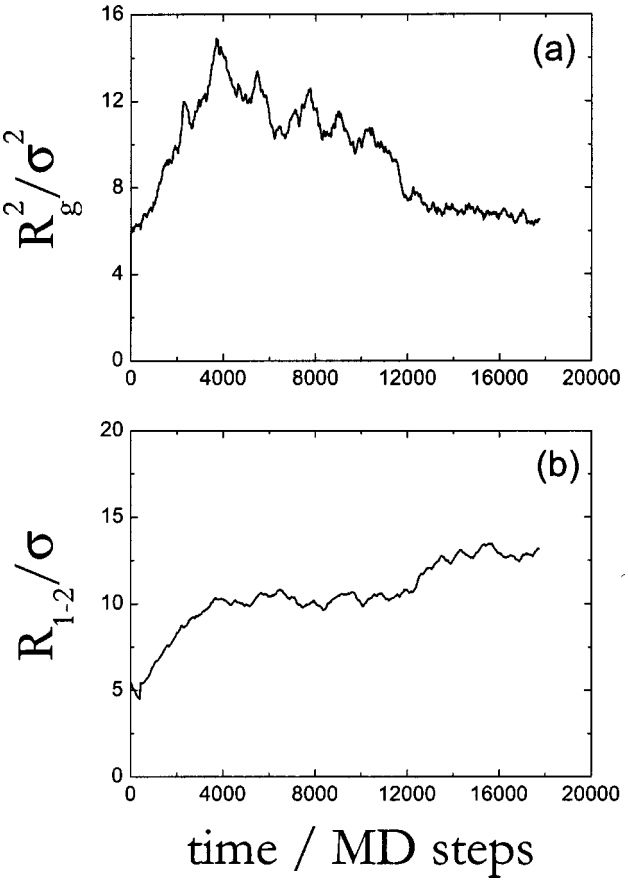

FIG. 16. Evolution of (a) the squared radius of gyration of the individual chain, R_g^2, and (b) the distance between the center-of-mass of the chains, R_{1-2} for the conditions illustrated by Fig. 15.

coupled to a heat bath by stochastic forces [see Eq. (5)]. This, of course, is only a drastic simplification of the possible aggregation scenario, but the qualitative conclusions that will be drawn are expected to be valid in general.

It is clear that the repulsive Coulomb forces acting between noncompensated charges on the chains attempt to disrupt the polymer ''droplet,'' while the surface tension tries to keep it spherical. In fact, this situation is almost the same as that observed by Lord Rayleigh for highly charged liquid droplets. It is well-known that, depending on the droplet radius and surface tension (or temperature), the electrified droplet can become unstable, i.e., it starts to deform into an elongated ellipsoid. Such a deformation can finally lead to a fission of the droplet into two fragments of equal size and charge, if the repulsive force between the like elementary charges on the surface exceeds the forces from surface tension. Here we record the dynamics of the disintegration process of two coalesced charged globules (polyion droplet) in the presence of counterions.

Sequence of images, which illustrates the evolution of the system after switching on the Coulomb interaction and a short relaxation period, is shown in Fig. 15, where, for visual clarity, we present three-dimensional Connolly surfaces[43,44] constructed for the polymer beads and do not depict the counterions. In Fig. 16 we present the evolution of the squared radius of gyration of the individual chain, R_g^2, and the distance between the center-of-mass of the chains, R_{1-2}.

From Fig. 15 we first observe, upon switching on the Coulomb repulsion, a deformation of the spherical polyion droplet into an elongated ellipsoid [which is distinctly seen in Figs. 15(a) and 15(b)] and then a splitting of the ellipsoid into a dumbbell-type structure [Figs. 15(c) and 15(d)], accompanied by a sharp increase in the chain's gyration radius [Fig. 16(a)]. Also, we observe an increase in the R_{1-2} value, indicating that two chains tend to segregate [Fig. 16(b)]. This process is very fast. As it is obvious from Fig. 16, it takes about 4000 time–steps, i.e., $t\approx 40\tau$. When a series of configurations was displayed graphically, a distinctive droplet thinning was observed, which is more or less transitory and spatially localized. Such thinning, leading to the formation of a dumbbell aggregate, is clearly seen in Figs. 15(c) and 15(d), where simulation results for transitional region are presented. The long-range electrostatic interactions control the overall elongated shape of the aggregate to maintain linear structures, whereas the monomer distribution inside the ''pearls'' is controlled by the short-range hydrophobic attractions to adopt the nearly spherical shape. On the time scales of simulation, the dumbbell-type structure formed at this stage is quite long-living and in a sense is similar to a necklace globule predicted by Dobrynin *et al.*[36] for a single polyelectrolyte chain under poor solvent conditions. In our case, however, there is no common connectivity of all chain beads and, as a result of random thermal agitation, a further splitting is observed as well, leading finally to the formation of two separated globules [Figs. 15(e) and 15(f)]. There are moderately large thickening-thinning fluctuations before the disintegration of the dumbbell aggregate into two ''splinters''. For the model considered here, it happens after about

1.2×10^4 time–steps ($t\approx120\tau$). Of course, this type of behavior depends on the interactions involved, but it can be undoubtedly realized for highly charged polyions.

The results presented in this subsection confirm our conclusion drawn for the multichain system that in the regime II the charged proteinlike globules can be stable in a poor solvent with respect to the aggregation.

IV. CONCLUDING REMARKS

In the present work, we have reported molecular dynamics simulations of a salt-free solution of highly charged proteinlike hydrophobic–hydrophilic ($\mathcal{HP}$) copolymers in a pure solvent. The sequence of monomer units along the chain was taken as fixed (quenched disorder), so that the corresponding entropic term is missing. The electroneutral (hydrophobic) $\mathcal{H}$ units and the charged (hydrophilic) $\mathcal{P}$ units were present in equal proportion. The polymer chains and univalent counterions were immersed in a Langevin fluid. The parameters of short-range (hydrophobic) interactions between $\mathcal{H}$ and $\mathcal{P}$ chain sites were chosen to promote the collapse of hydrophobic units into a dense core shielded by charged $\mathcal{P}$ sites from the solvent. The processes of coil-to-globule transition, aggregation of copolymer globules, and counterion condensation were studied in detail as a function of temperature. We have found that both inter- and intramolecular interactions of hydrophobic and electrostatic type can compete and have a profound influence on the formation of stable proteinlike globules with a specific internal core-shell morphology as well as on their aggregation.

From the results of the simulations we have concluded that there are three different temperature regimes for the multichain system, which are characterized by a different behavior of Coulomb energy, chain size, and pair correlation functions describing the spatial distribution of $\mathcal{H}$ and $\mathcal{P}$ monomer units and counterions:

(i) In the high-temperature regime, at reduced temperature $T>3.0$ (the reduced Bjerrum length $l_B<1/3\sigma$), the copolymer chains have an extended coil-like conformation with many hydrophobic blobs. In this case, the presence of counterions, which are distributed almost uniformly in salt-free solution, can be neglected.

(ii) As temperature is decreased below $T\lesssim1.5$ (when the reduced Bjerrum length is of the order of the segment size, $l_B\gtrsim0.67\sigma$), counterion condensation begins together with a sharp decrease in chain size. In this case, however, there is still a large fraction of free counterions. The single proteinlike polyions can readily adopt compact conformations with the hydrophobic chain sections clustered at the globular core and the charged hydrophilic sections forming the envelope of this core and buffering it from polar solvent. However, in contrast to real protein native states, at the $\mathcal{HP}$ level of description used in our work, this specific core-shell morphology is not unique. In this intermediate temperature regime, we have observed a stable solution of nonaggregating polymer globules which are well-separated from each other and form an array of colloidlike particles. Each globule attracts charge-neutralizing counterions, which form surrounding clouds. Under these conditions, charged proteinlike copolymers should be soluble in a poor solvent. Although globules are strongly correlated due to the Coulombic interaction, their spacings are not regular and cannot be identified as a Wigner crystal. A solution of globules has also been seen in the molecular dynamics simulations of Kremer and co-workers,[23,24] who studied highly charged regular copolymers in a poor solvent.

It should be stressed that the situation discussed in the present work is different from the case of solutions of weakly charged polyelectrolytes in a poor solvent which can form microphase-separated structures with alternating polymer-rich and polymer-poor regions.[45] In these regions, the condition of electroneutrality is violated locally at a cost in electrostatic energy but the gain in translational entropy of the mobile counterions is sufficient to stabilize such microstructures.[45]

(iii) A further decrease in temperature ($T\lesssim0.4\div0.5$ or $l_B\gtrsim2\sigma$) leads to the condensation of most of the counterions and the aggregation of dense proteinlike globules. However, no large-scale aggregation formation is observed. At the lowest temperature considered in the simulation, $T=0.25$, about 90% of the counterions are condensed on non-neutral sites of the globules, while the rest are still floating in the space, indicating that ~10% bare charges remain on the globules. We have found that the main driving force for the aggregation is short-range attractive hydrophobic interaction between chain sites. The aggregation of like-charged globules leads to the formation of a specific multiglobular structure built up from stable individual globules connected by the condensed counterion layers. It has been shown that the mesoscopic globular aggregates have a chainlike morphology due to repulsion between non-compensated charges on single collapsed chains. In the thermodynamic limit, the aggregation and the subsequent phase separation would be observed.

The transitions between the three temperature regimes have been found to be thermodynamically reversible.

In the literature, there are some experimental results confirming the trends observed in our simulations.

Recently, Peng and Wu[46] have studied an aqueous solution of charge-stabilized cross-linked microgels and linear (noncross-linked) chains prepared by copolymerization of N-vinylcaprolactam and sodium acrylate, P(VCL-*co*-NaA). For linear chains under poor solvent conditions in the presence of univalent counterions Na^+, they observed a temperature-induced coil-to-globule transition of the chain conformation, leading to a single-chain core-shell nanostructure in which negatively charged COO^- groups are concentrated in the solution-exposed part of the globule (the same core-shell morphology was observed for the cross-linked microgels). In the temperature range studied, it was found that the average hydrodynamic radius and the average monomer density for the linear P(VCL-*co*-NaA) chains and spherical microgels gradually decrease as the solvent becomes poorer, but neither the apparent weight-average molar mass and the average number of aggregation change, clearly indicating that there is no intermolecular aggregation for both the collapsed linear chains and contracted microgels. The existence of these stable nonaggregating states in a dilute solution ($\sim10^{-6}$ g/mol) was attributed to a balance between hydrophobic attraction and strong electrostatic repulsion in the

compact core-shell conformations formed in a poor solvent by the P(VCL-*co*-NaA) copolymer at sufficiently high content of ionizable acrylic groups. These results are in good qualitative agreement with our findings corresponding to the regimes I and II, when charged proteinlike copolymers are soluble due to the large net charge of each chain.

It is known that, depending on the primary amino acid sequence of proteins, there are two possible scenarios of protein aggregation in solution, when the attractive hydrophobic interaction dominates over the stabilizing electrostatic repulsion as the net charge of the protein is reduced. In the first case, globular proteins are able to form stable aggregates (dimmers, trimers, etc.) maintaining in general their native conformations which they have in the low-concentration limit. The self-association and dimerization of lysozime, experimentally studied for a considerable time,[47–49] is a typical example of this scenario. In the second case, proteins can also aggregate, but, in order to gain the maximum potential energy and to form the most stable structure, they should refold into a conformation dissimilar from the native (single-chain) state, the aggregation scenario suggested, e.g., for the cellular prion protein PrP,[50,51] capable of converting from the PrP^{c} form with α-helices into the PrP^{sc} misfolded structure having β-sheets. It can be assumed that our simple model of the charged proteinlike copolymers under conditions corresponding to the regime III reflects some general features of the aggregative processes observed for real proteins in the framework of the first scenario described above.

ACKNOWLEDGMENTS

The financial support from the Alexander-von-Humboldt Foundation, Program for Investment in the Future (ZIP), INTAS (project # 01-607), and Russian Foundation for Basic Research is greatly appreciated. D.A.M. acknowledges the ''Deutscher Akademischer Austauschdienst'' (DAAD) for financial support.

[1] C. Branden and J. Tooze, *Introduction to Protein Structure*, 2nd ed. (Garland Publishing, Inc., New York, 1999).
[2] I. M. Lifshitz, A. Yu. Grosberg, and A. R. Khokhlov, Rev. Mod. Phys. **50**, 683 (1978).
[3] A. Yu. Grosberg and A. R. Khokhlov, *Statistical Physics of Macromolecules* (American Institute of Physics, New York, 1994).
[4] A. R. Khokhlov and P. G. Khalatur, Physica A **249**, 253 (1998).
[5] P. G. Khalatur, V. I. Ivanov, N. P. Shusharina, and A. R. Khokhlov, Russ. Chem. Bull. **47**, 855 (1998).
[6] A. R. Khokhlov and P. G. Khalatur, Phys. Rev. Lett. **82**, 3456 (1999).
[7] V. A. Ivanov, A. V. Chertovich, A. A. Lazutin, N. P. Shusharina, P. G. Khalatur, and A. R. Khokhlov, Macromol. Symp. **146**, 259 (1999).
[8] E. A. Zheligovskaya, P. G. Khalatur, and A. R. Khokhlov, Phys. Rev. E **59**, 3071 (1999).
[9] J. M. P. van den Oever, F. A. M. Leermakers, G. J. Fleer, V. A. Ivanov, N. P. Shusharina, A. R. Khokhlov, and P. G. Khalatur, Phys. Rev. E **65**, 041708 (2002).
[10] Yu. A. Kriksin, P. G. Khalatur, and A. R. Khokhlov, Macromol. Theory Simul. **11**, 213 (2002).
[11] A. V. Chertovich, V. A. Ivanov, B. G. Zavin, and A. R. Khokhlov, Macromol. Theory Simul. **11**, 751 (2002).
[12] E. N. Govorun, V. A. Ivanov, A. R. Khokhlov, P. G. Khalatur, A. L. Borovinsky, and A. Yu. Grosberg, Phys. Rev. E **64**, 040903 (2001).
[13] J. Virtanen, C. Baron, and H. Tenhu, Macromolecules **33**, 336 (2000); J. Virtanen and H. Tenhu, Macromolecules **33**, 5970 (2000).
[14] V. I. Lozinsky, I. A. Simenel, E. A. Kurskaya, V. K. Kulakova, V. Ya. Grinberg, A. S. Dubovik, I. Yu. Galaev, B. Mattiasson, and A. R. Khokhlov, Rep. Russ. Acad. Sci. **375**, 637 (2000); P.-O. Wahlund, I. Yu. Galaev, S. A. Kazakov, V. I. Lozinsky, and B. Mattiasson, Macromol. Biosci. **2**, 33 (2002); M.-H. Siu, G. Zhang, and C. Wu, Macromolecules **35**, 2723 (2002).
[15] M. Stevens and K. Kremer, J. Chem. Phys. **103**, 1669 (1995).
[16] R. G. Winkler, M. Gold, and P. Reineker, Phys. Rev. Lett. **80**, 3731 (1998).
[17] J. C. Chu and C. H. Mak, J. Chem. Phys. **110**, 2669 (1999).
[18] P. Chodanowski and S. Stell, J. Chem. Phys. **111**, 6069 (1999).
[19] N. Lee and D. Thirumalai, Macromolecules **34**, 3446 (2001).
[20] H. J. Limbach, C. Holm, and K. Kremer, Europhys. Lett. **60**, 566 (2002).
[21] R. G. Winkler, M. O. Steinhauser, and P. Reineker, Phys. Rev. E **66**, 021802 (2002).
[22] R. Chang and A. Yethiraj, J. Chem. Phys. **116**, 5284 (2002).
[23] U. Micka, C. Holm, and K. Kremer, Langmuir **12**, 4033 (1999).
[24] U. Micka and K. Kremer, Europhys. Lett. **49**, 189 (2000).
[25] K. F. Lau and K. A. Dill, Macromolecules **22**, 3986 (1989).
[26] K. F. Lau and K. A. Dill, Proc. Natl. Acad. Sci. U.S.A. **87**, 6388 (1990).
[27] P. P. Ewald, Ann. Phys. (Leipzig) **64**, 253 (1921).
[28] M. P. Allen and D. J. Tildesley, *Computer Simulation of Liquids* (Claredon, Oxford, 1990).
[29] T. A. Darden, D. M. York, and L. G. Pedersen, J. Chem. Phys. **98**, 10089 (1993).
[30] U. Essmann, L. Perera, M. L. Berkowitz, T. Darden, H. Lee, and L. G. Pedersen, J. Chem. Phys. **103**, 8577 (1995).
[31] H. C. Andersen, J. Comput. Phys. **52**, 24 (1983).
[32] L. Wesson and D. Eisenberg, Protein Sci. **1**, 227 (1992).
[33] J. D. Augspurger and H. A. Scheraga, J. Comput. Chem. **17**, 1549 (1996).
[34] H. Schiessel and P. Pincus, Macromolecules **31**, 7953 (1998).
[35] H. Schiessel, Macromolecules **32**, 5673 (1999).
[36] A. V. Dobrynin, M. Rubinstein, and S. P. Obukhov, Macromolecules **29**, 2974 (1996).
[37] F. J. Solis and M. Olvera de la Cruz, Macromolecules **31**, 5502 (1998).
[38] A. R. Khokhlov and E. Yu. Kramarenko, Macromolecules **29**, 681 (1996).
[39] N. Th. M. Klooster, F. van der Touw, and M. Mandel, Macromolecules **17**, 2070 (1984); **17**, 2078 (1984); **17**, 2087 (1984).
[40] S. G. Starodoubtsev, A. R. Khokhlov, E. L. Sokolov, and B. Chu, Macromolecules **28**, 3930 (1995).
[41] G. S. Manning, J. Chem. Phys. **51**, 924 (1969).
[42] J. Ray and G. S. Manning, Langmuir **10**, 2450 (1994).
[43] A Connolly surface (Ref. 44) is the locus of points formed by the intersection of the surface of a given ensemble of particles with a spherical probe particle of radius r_p, which is rolled over the particles belonging to the system under consideration. In this way, the molecular surface distribution (of radius r_s=particle radius+probe radius) can be obtained with the probe radius as a parameter. In our calculations, we set $r_p=\sigma$.
[44] M. L. Connolly, Science **221**, 709 (1983).
[45] V. Yu. Borue and I. Ya. Erukhimovich, Macromolecules **23**, 3625 (1990).
[46] S. Peng and C. Wu, J. Phys. Chem. **105**, 2331 (2001).
[47] A. J. Sophianopoulos and K. E. V. Holde, J. Biol. Chem. **239**, 2516 (1964).
[48] F. Wang, J. Hayter, and L. J. Wilson, Acta Crystallogr., Sect. D: Biol. Crystallogr. **52**, 901 (1996).
[49] D. R. Booth *et al.*, Nature (London) **385**, 787 (1997).
[50] S. B. Prusiner, Science **252**, 1515 (1991).
[51] F. E. Cohen, K.-M. Pan, Z. Huang, M. Baldwin, R. Fletterick, and S. B. Prusiner, Science **264**, 530 (1994).